One dimensional Kronig-Penney model with positional disorder: Theory versus experiment

G. A. Luna-Acosta and F. M. Izrailev
Instituto de Física, Universidad Autónoma de Puebla, Apartado Postal J-48, Puebla 72570, Mexico

N. M. Makarov
Instituto de Ciencias, Universidad Autónoma de Puebla, Priv. 17 Norte No. 3417, Col. San Miguel Hueyotlipan, Puebla 72050, Mexico

U. Kuhl and H.-J. Stöckmann
Fachbereich Physik der Philipps–Universität Marburg, Renthof 5, D-35032 Marburg, Germany
(Received 22 June 2009; revised manuscript received 7 August 2009; published 15 September 2009)

We study the effects of random positional disorder in the transmission of waves in the one-dimensional Kronig-Penny model formed by two alternating dielectric slabs. Numerical simulations and experimental data revealed that the so-called resonance bands survive even for relatively strong disorder and large number of cells, while the nonresonance bands disappear already for weak disorder. For weak disorder we derive an analytical expression for the localization length and relate it to the transmission coefficient for finite samples. The obtained results describe very well the experimental frequency dependence of the transmission in a microwave realization of the model. Our results can be applied both to photonic crystals and semiconductor superlattices.

DOI: 10.1103/PhysRevB.80.115112 PACS number(s): 72.15.Rn, 42.25.Bs, 42.70.Qs

I. INTRODUCTION

In recent years there is a high activity in the study of wave (electron) propagation through one-dimensional (1D) periodic structures (see, for example, Ref. 1 and references therein). Much is already known about band structures of perfectly propagating waves in strictly periodic and relatively simple devices and one of the current interests is the influence of random imperfections that are commonly present in real experiments. These imperfections are originated, for example, from the variations in the medium parameters such as the dielectric constant, magnetic permeability, and barrier widths or heights[2–9].

The analysis of scattering properties of periodic-on-average (when periodic systems are slightly affected by a disorder) models with various kinds of disorder is mainly related to numerical methods. It is obvious that giving important results for specific models and parameters, the numerical approaches cannot serve as a guide for the understanding of generic properties caused by disorder. In this paper we try to fill this gap in the theory by the derivation of the localization length for the 1D Kronig-Penney model, relating it to the properties of transmission through a finite number of disordered barriers.

Our analytical results are compared with the experimental data obtained for a single-mode microwave guide. We show that in spite of the standard restrictions of analytical results (restricted to infinite samples and weak disorder), comparison between theory and experiment is quite good. This fact is highly nontrivial since the experimental data are strongly influenced by absorption in the waveguide walls, an effect that is also not taken into account analytically.

Our study is relevant to other types of 1D stratified media, for example, to electron transport through random superlattices[10] (disordered arrays of semiconductor quantum wells/barriers) or acoustic waves in random layered media[11]. Also, similar properties of the transmission are expected to occur in the 1D *quantum* Kronig-Penney model (with alternating rectangular wells and barriers).

In Sec. II the model is specified and the transfer matrix equations are derived. In Sec. III the experimental setup is briefly discussed and the numerical simulations for the transmission coefficient are compared with experimental results for the case of an array of 26 cells and different amounts of positional disorder. In Sec. IV we present the main experimental results and discuss some of the properties of transmission. In Sec. V we derive, for the regime of weak disorder, the analytical expression for the logarithm of the transmission in connection with the inverse localization length. We compare there too the numerical simulations and analytical results with the experimental data and show the effectiveness of our analytical approach. In Sec. VI, we summarize our results.

II. MODEL

We consider an array formed by two alternating dielectric slabs with refractive indices n_a and n_b placed in an electromagnetic metallic-wall waveguide of constant width w and height h; see Fig. 1. For convenience, the layers with the refractive index $n_a(n_b)$ shall be referred as to the a layers (b layers). The lengths of the nth a and b layers are denoted,

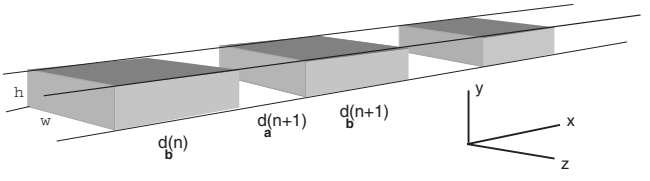

FIG. 1. Kronig-Penney model with Teflon bars of constant length $d_b(n)=d_b(n+1)=d_b$ and air spacings $d_a(n)$ defined by Eq. (2.1).

respectively, by $d_a(n)$ and $d_b(n)$. The positional disorder in our model consists in randomly varying lengths of *only* one type of layer, say the a layer, such that

$$d_a(n) = d_a + \sigma\eta(n), \quad \langle d_a(n)\rangle = d_a, \quad d_b(n) = d_b. \quad (2.1)$$

Here σ is rms deviation of $d_a(n)$ and σ^2 its variance. Hence, $\eta(n)$ is a sequence with zero average and unit variance. In this work we assume that $\eta(n)$ is random uncorrelated, i.e.,

$$\langle \eta(n)\eta(n')\rangle = \delta_{nn'}, \quad \langle \eta(n)\rangle = 0. \quad (2.2)$$

The angular brackets $\langle \ldots \rangle$ stand for a statistical average over different realizations of randomly layered structure. Note that the random structure is *periodic on average* with the period $d=d_a+d_b$.

In this work we shall treat the lowest TE mode of frequency ν whose electric field $\mathbf{E}$ is defined by

$$E_y = \sin(\pi z/w)\Psi(x), \quad E_x = E_z = 0 \quad (2.3)$$

(see Fig. 1). Within every a or b layer, the function $\Psi(x)$ obeys the 1D Helmholtz equation,

$$\left(\frac{d^2}{dx^2} + k_{a,b}^2\right)\Psi_{a,b}(x) = 0, \quad (2.4)$$

with the wave numbers

$$k_{a,b} = \frac{2\pi}{c}\sqrt{n_{a,b}^2\nu^2 - (c/2w)^2}. \quad (2.5)$$

In the incoming-outgoing wave representation, the solution of Eq. (2.4) for the nth elementary cell reads

$$\Psi_{a_n}(x) = A_n^+ \exp\{ik_a[x - x_a(n)]\} + A_n^- \exp\{-ik_a[x - x_a(n)]\} \quad (2.6)$$

inside the a_n layer, $x_a(n) \le x \le x_b(n)$, and

$$\Psi_{b_n}(x) = B_n^+ \exp\{ik_b[x - x_b(n)]\} + B_n^- \exp\{-ik_b[x - x_b(n)]\} \quad (2.7)$$

inside the b_n layer, $x_b(n) \le x \le x_a(n+1)$. Here $A_n^\pm$ and $B_n^\pm$ are complex amplitudes of the forward/backward traveling wave; the coordinates $x_a(n)$ and $x_b(n)$ denote the left-hand boundaries of the a_n and b_n layers, respectively.

With the use of the continuity conditions for the wave function $\Psi_{a,b}(x)$ and its derivative at the boundaries $x = x_b(n)$ and $x = x_a(n+1)$ one can obtain the transfer relation for the amplitudes $A_{n+1}^\pm$ and $A_n^\pm$ of two adjacent cells,

$$\begin{pmatrix} A_{n+1}^+ \\ A_{n+1}^- \end{pmatrix} = \begin{pmatrix} Q_{11}(n) & Q_{12}(n) \\ Q_{21}(n) & Q_{22}(n) \end{pmatrix}\begin{pmatrix} A_n^+ \\ A_n^- \end{pmatrix}. \quad (2.8)$$

The transfer matrix $\hat{Q}(n)$ has the following elements:

$$Q_{11}(n) = [\cos(k_b d_b) + i\alpha_+ \sin(k_b d_b)]\exp[ik_a d_a(n)] = Q_{22}^*(n), \quad (2.9a)$$

$$Q_{12}^*(n) = i\alpha_- \sin(k_b d_b)\exp[ik_a d_a(n)] = Q_{21}(n). \quad (2.9b)$$

Here the asterisk stands for the complex conjugation and we introduced the parameters $\alpha_\pm$,

$$\alpha_\pm = \frac{1}{2}\left(\frac{k_a}{k_b} \pm \frac{k_b}{k_a}\right), \quad \alpha_+^2 - \alpha_-^2 = 1. \quad (2.10)$$

The determinant of $\hat{Q}(n)$ is equal to unit, $\det \hat{Q}(n) = 1$. Note that the transfer matrix $\hat{Q}(n)$ differs from cell to cell only in the phase factor $\exp[ik_a d_a(n)]$.

The transfer matrix equation for the array of N cells with or without positional disorder is

$$\begin{pmatrix} A_{N+1}^+ \\ A_{N+1}^- \end{pmatrix} = \hat{Q}^N \begin{pmatrix} A_1^+ \\ A_1^- \end{pmatrix}, \quad (2.11)$$

where

$$\hat{Q}^N = \hat{Q}(N)\hat{Q}(N-1)\ldots\hat{Q}(n)\ldots\hat{Q}(2)\hat{Q}(1). \quad (2.12)$$

All matrices $\hat{Q}(n)$ $(n=1,2,\ldots,N)$ have the same form (2.9), only differing in the values of $d_a(n)$. In our following numerical simulations and experimental setup we have $A_{N+1}^- = 0$. Thus, the transmittance of N cells is given by

$$T_N \equiv |A_{N+1}^+/A_1^+|^2 = |Q_{11}^N|^{-2} = |S_{12}^N|^2, \quad (2.13)$$

where S_{12}^N is the scattering matrix element in the relation

$$\begin{pmatrix} A_1^- \\ A_{N+1}^+ \end{pmatrix} = \begin{pmatrix} S_{11}^N & S_{12}^N \\ S_{21}^N & S_{22}^N \end{pmatrix}\begin{pmatrix} A_1^+ \\ A_{N+1}^- \end{pmatrix}. \quad (2.14)$$

In the case of *no disorder*, $\eta(n)=0$, the length of a layer does not depend on the cell number n, $d_a(n)=d_a$. Therefore, the unperturbed transfer matrix $\hat{Q}^{(0)}$ is described by Eq. (2.9) with $d_a(n)$ replaced by the constant length d_a. As is known (see, e.g., Ref. 1), the transmission through N *identical* cells is expressed in closed form as

$$T_N^{(0)} = \frac{1}{1 + \left|Q_{12}^{(0)}\dfrac{\sin(N\kappa d)}{\sin(\kappa d)}\right|^2} = |S_{12}^{(0)N}|^2, \quad (2.15)$$

where κ is the Bloch wave number defined by the dispersion relation

$$\cos(\kappa d) = \cos(k_a d_a)\cos(k_b d_b) - \alpha_+ \sin(k_a d_a)\sin(k_b d_b). \quad (2.16)$$

Expression (2.15) indicates that the transmission is perfect $(S_{12}^{(0)N}=1)$ for all N when $Q_{12}^{(0)} = -i\alpha_- \sin(k_b d_b) = 0$ or $\sin(N\kappa d)/\sin(\kappa d) = 0$. The former occurs at the Fabry-Perot resonances $k_b d_b = m\pi$ in the b layers. The latter produces $N-1$ Fabry-Perot oscillations in each spectral band associated with the total system length Nd. We shall refer to the resonances $k_b d_b = m\pi$ as "Teflon resonances" since in the experiment the b slabs are made of Teflon, whereas the a slabs are just air.

III. EXPERIMENTAL SETUP

In Fig. 2 we show the experimental setup of a microwave ring guide of height $h=1$ cm, width $w=2$ cm, and perimeter $P=234$ cm. The waveguide consists of $N=26$ cells, where

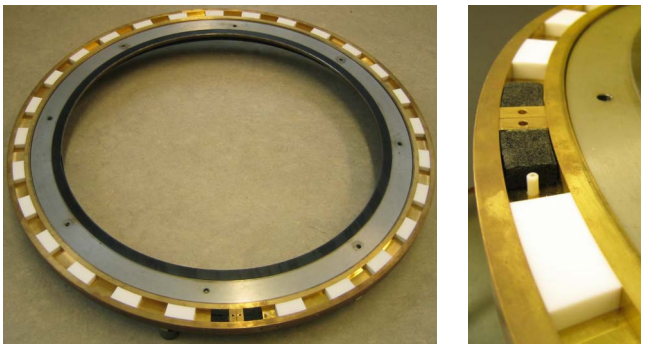

FIG. 2. (Color online) The microwave guide. Left: overview of the brass waveguide of perimeter $P=234$ cm with height $h=1$ cm and width $w=2$ cm. Right: an enlargement of the waveguide showing the two carbon pieces (black) and one of the electric dipole antennas. The other lies on a brass lid (not shown) inserted near the other carbon piece. The white pieces are the Teflon bars.

the b layers are pieces of Teflon of length $d_b=4.078$ cm and the refractive index $n_b=\sqrt{2.08}$. Two electric dipole antennas connect to a network analyzer. Also shown are the two carbon pieces used to absorb the electric field at both ends of the waveguide and thus mimic two infinite leads connected to each side of the array of Teflon pieces and air segments. The frequency range is 7.5–15 GHz corresponding to wavelengths from 4 to 2 cm. This arrangement has been used to study the transport effects of single impurities in the photonic Kronig-Penny model[12]. Earlier, in an analogous model with metallic screws instead of Teflon pieces, the microwave realization of the Hoftstadter butterfly[13] was studied. The same configuration (metallic screws) was used to investigate transport properties of on-site correlated disorder[14–16].

Obviously this waveguide is not rectilinear; in the experiment the Teflon pieces and air segments are not perfect parallelepipeds: one side is longer than the other by 5%. However, since the perimeter (234 cm) is much larger than the wavelength of the electric field even in the regime of the first mode, it is expected that the rectilinear model is a good approximation. In fact, as shown in detail in Ref. 12, a good quantitative agreement is found by defining an effective length of the Teflon pieces and the air segments that are 1.95% larger than the smaller side of the Teflon pieces and air segments. For example, the length of the smaller (inner) length of the Teflon pieces used in the experiments reported here is 4 cm, so the effective width d_b we use in our calculations is 4.078 cm. We remark that this value is found by best fitting and is the only fitting, good for the whole frequency range of all our results presented here.

In Fig. 3, curve (a), we plot the experimentally measured value of $|S_{12}^N|$ (in what follows, the *transmission spectrum*) for the 26-cell *periodic array*. Curve (c) is the transmission spectrum $|S_{12}^{(0)N}|$ calculated according to Eqs. (2.15) and (2.16) and unperturbed Eq. (2.9). Note that the experimental transmission spectrum is about 1/5 of the theoretical one. This decrease in the signal is due to absorption in the metallic walls of the waveguide coming from the skin effect. Additionally, the coupling of the antenna varies slightly with frequency giving rise to small oscillations of the transmission spectrum on a large frequency scale. Our question is the global frequency dependence of the transmission spectrum on the frequency giving us a possibility to reveal resonance effects and the role of disorder. Note that the band structure of the spectrum remains practically the same in spite of a strong absorption (see discussion in Refs. 14–16).

Inspection of the transmission spectrum $|S_{12}^{(0)N}|$ of the perfectly periodic array, Fig. 3, curve (c), demonstrates the effect of the Teflon resonances on the transmission bands. We see two types of bands; namely, bands 1, 2, 4, and 6 show the $N-1=25$ oscillations mentioned above, whereas bands 3, 5,

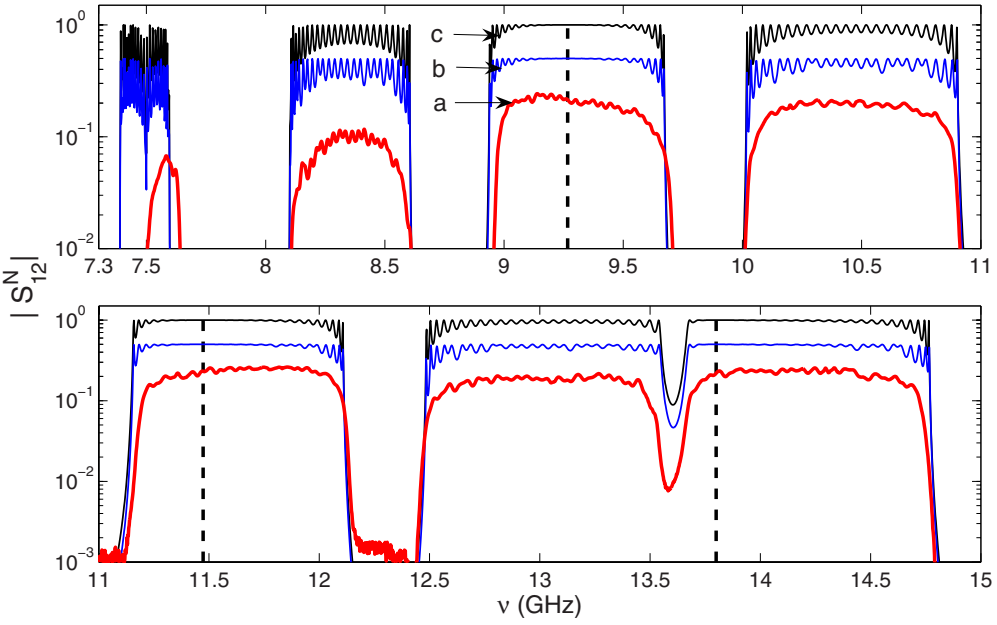

FIG. 3. (Color online) Transmission spectrum for a 26-cell array. Top: $7.3<\nu<11$ GHz. Bottom: $11<\nu<15$ GHz. Curve (a): experimental data for the periodic array. Curve (b): $|S_{12}^N|$, multiplied by 1/2, for a slightly random ($\epsilon=0.049$) array. Curve (c): $|S_{12}^{(0)N}|$ for the perfectly periodic array ($d_a=d_b=4.078$ cm). Dashed vertical lines mark the position of the Teflon resonances.

and 7 are flat ($|S_{12}^{(0)N}| \approx 1$) around the resonance since $|Q_{12}^{(0)}|$ is zero at the resonance and very small in some neighborhood around it. For future reference we shall refer to the second type of bands as the "resonance bands." Clearly, these bands disappear when $d_b \to 0$, turning into those with $N-1$ oscillations occurring for delta-function potentials.

In accordance with Eq. (2.5), the first (lowest) mode in the *air spacings* (a slabs) opens at the cutoff frequency $\nu_a^{\text{cut}} = (c/2wn_a) = 7.5$ GHz while in the *Teflon b* layers it opens at $\nu_b^{\text{cut}} = (c/2wn_b) = 5.2$ GHz, which is less than $\nu_a^{\text{cut}} (n_a < n_b)$. On the other hand, Fig. 3 specifies the bottom of the first transmission band at $\nu_1^{\text{bot}} = 7.387$ GHz. So that the real cutoff ν_1^{bot} pertains to the interval $\nu_b^{\text{cut}} < \nu_1^{\text{bot}} < \nu_a^{\text{cut}}$ where the wave number k_a in the air spacings is purely imaginary, $k_a = i(2\pi/c)\sqrt{(c/2w)^2 - \nu^2}$. The transmission in this regime is due to tunneling through the air spacings. This fact makes the profile of the first band [see Fig. 3, curve (c)] somewhat special: there is a dip in the transmission band right at the frequency where the first mode opens in the air.

Note that except for the first band, the positions and widths of the transmission gaps as well as the band profiles of the experimental curve are well reproduced by the transfer matrix calculations (2.13). The discrepancy for the first band is understood since for low frequencies the wavelength is not sufficiently small compared to the perimeter of the circular waveguide, and hence the rectilinear waveguide model fails. For the second and higher bands, the agreement is better and the experimental curve does show some evidence of the small $N-1$ band oscillations predicted by the model. Clearly, these do not appear as perfectly regular oscillations and this irregularity may be caused by experimental imperfections due to variations in the length and positions of the Teflon pieces.

The maximum deviation $|d_b(n) - d_b|_{\max}$ in the length of the Teflon pieces is about 0.01 cm and the maximum deviation $|d_a(n) - d_a|_{\max}$ in the air spacings, due to the placement of the Teflon pieces, is estimated to be about 0.04 cm. Are imprecisions of this order sufficient to break the regularity of the oscillations?

To check this, we performed a simulation with a disordered sequence assuming $|d_a(n) - d_a|_{\max} = 0.04$ cm and an error described by a random sequence $\eta(n)$ with a uniform random distribution in accordance with Eqs. (2.1), (2.2), (2.12), and (2.13). The result is plotted in Fig. 3, curve (b). This curve has been multiplied by 0.5 in order to show it together with the perfectly regular case and the experimental data. Inspection shows that indeed the assumed small error is enough to break the regularity of the band oscillations giving a better agreement with the experimental data of the supposedly regular array.

IV. DISORDERED ARRAY

Let us now move to intentionally disordered arrays, with the lengths of all Teflon bars constant, $d_b(n) = d_b$ while the air layers have random lengths given by Eqs. (2.1) and (2.2). In our experimental and numerical calculations, the sequence $\eta(n)$ is an uncorrelated random function uniformly distributed in the interval $[-\sqrt{3}, \sqrt{3}]$, with unit variance.

TABLE I. Parameter values of random disorder. Here $d = d_a + d_b = 2d_a \approx 8.16$ cm.

Case	$\epsilon / 10^{-2}$	$\frac{\sigma}{d} (= \frac{\epsilon}{\sqrt{3}})$	$(\frac{\sigma}{d})^2$
Very weak	0.49	0.28×10^{-2}	8.0×10^{-6}
Weak	3.00	1.77×10^{-2}	3.0×10^{-4}
Medium	12.30	7.07×10^{-2}	5.0×10^{-3}
Strong	49.00	28.30×10^{-2}	8.0×10^{-2}

A priori it is not known how large a random deviation from the average value d_a should be to observe weak, medium, or strong disorder effects in the transmission. We tentatively classify the amount of disorder by the value of the maximum deviation from the average length of the air spacing divided by the average length of the cells,

$$\epsilon \equiv \frac{|d_a(n) - d_a|_{\max}}{d} = \sigma\sqrt{3}/d. \tag{4.1}$$

Table I shows the values of ϵ we consider in this work together with corresponding values of relative rms σ/d and $(\sigma/d)^2$. The latter quantity is needed to ease the comparison with analytical results obtained below. The case of $\epsilon = 0.49 \times 10^{-2}$ was discussed above to simulate the errors in the experimental setup. We call it the case of extremely weak disorder. Similarly, $\epsilon = 3.0 \times 10^{-2}$, 12.3×10^{-2}, and 49.0×10^{-2}, respectively, are called the weak, medium, and strong disordered cases.

Figure 4 shows the transmission for the array of 26 cells with the positional disorder. Compared with the case of weak disorder [Fig. 4(a)], for medium disorder [Fig. 4(b)] only the first two gaps are clearly distinguishable; the third only partially. There is no trace of the $N-1$ oscillations in the transmission bands, and the second, fourth, and sixth transmission bands have decayed substantially. However, remnants of the *resonance bands* are still recognized and so this can be considered the regime of medium disorder. For strong disorder [Fig. 4(c)] the first two transmission bands have disappeared. There is no longer any evidence of the band structure of the unperturbed array. But still the transmission spectrum is close to one in the vicinity of the Teflon resonances. Close inspection of the plots of Fig. 4 shows that the transmission spectrum fluctuates more rapidly for the transfer matrix calculations [Eq. (2.13)] than for the experimental data. In the experiment the fast oscillations are suppressed by absorption. Moreover, the exact pattern of the oscillations is strongly dependent on the particular realization of the random disorder for a given value of the rms deviation σ. Although the random sequence $\eta(n)$ used in the transfer matrix calculations was implemented in the experimental setup, small unavoidable differences in $\eta(n)$ contribute to the observed differences in some of the oscillations. However, in general the main oscillations are well reproduced by the transfer matrix calculations.

The results so far discussed pertain to the array of $N = 26$ cells so the question arises about the effects on larger arrays. Our experimental setup does not allow for the implementation of much larger arrays. However, given that the

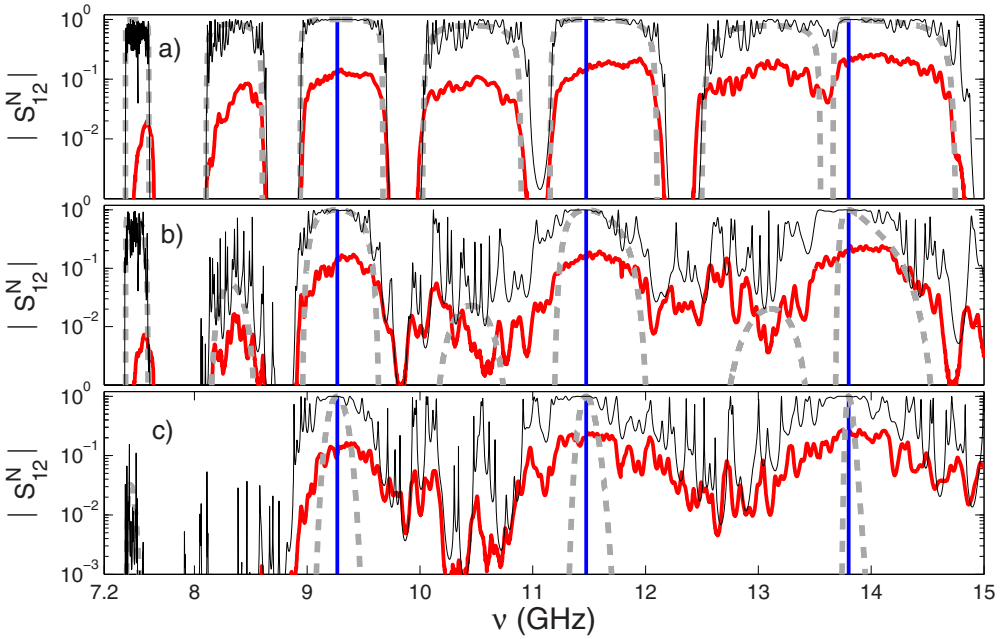

FIG. 4. (Color online) Transmission spectrum $|S_{12}^N|$ for 26-cell arrays: (a) weak ($\epsilon=3.0\times10^{-2}$), (b) medium ($\epsilon=12.3\times10^{-2}$), and (c) strong disorder ($\epsilon=49.0\times10^{-2}$). Transfer matrix calculations are shown by thin black solid curves and experimental measurements by thick red solid curves. Dashed curves correspond to analytical expression (5.18) for the inverse localization length. Perpendicular lines mark the position of the Teflon resonances.

transfer matrix calculations (2.13) are in good agreement with the experimental data for $N=26$ cells, we now consider only numerically, and later analytically, larger arrays for the same three cases: weak, medium, and strong disorder.

In Figs. 5(a)–5(c) we plot $|S_{12}^N|$ for an array with $N=100$ cells, for weak [Fig. 5(a)], medium [Fig. 5(b)], and strong [Fig. 5(c)] disorder. Similarly, in Figs. 5(d)–5(f) we plot $|S_{12}^N|$ for an array with $N=400$ cells, again for weak [Fig. 5(d)], medium [Fig. 5(e)], and strong [Fig. 5(f)] disorder. Comparing, for example, Figs. 5(a) and 5(d), corresponding to weak disorder for $N=100$ and $N=400$ cells, respectively, we see that the effect of increasing the size of the array, keeping the same amount of disorder, is to further decrease the transmission, consistent with the localization theory. However, this decrease occurs only away from the Teflon resonance frequencies. For medium and strong disorder, transmission has decayed below 10^{-3} for most of the frequencies except around the Teflon resonances. Thus, the localization is not homogeneous at all: the Teflon Fabry-Perot resonances strongly suppress the localization.

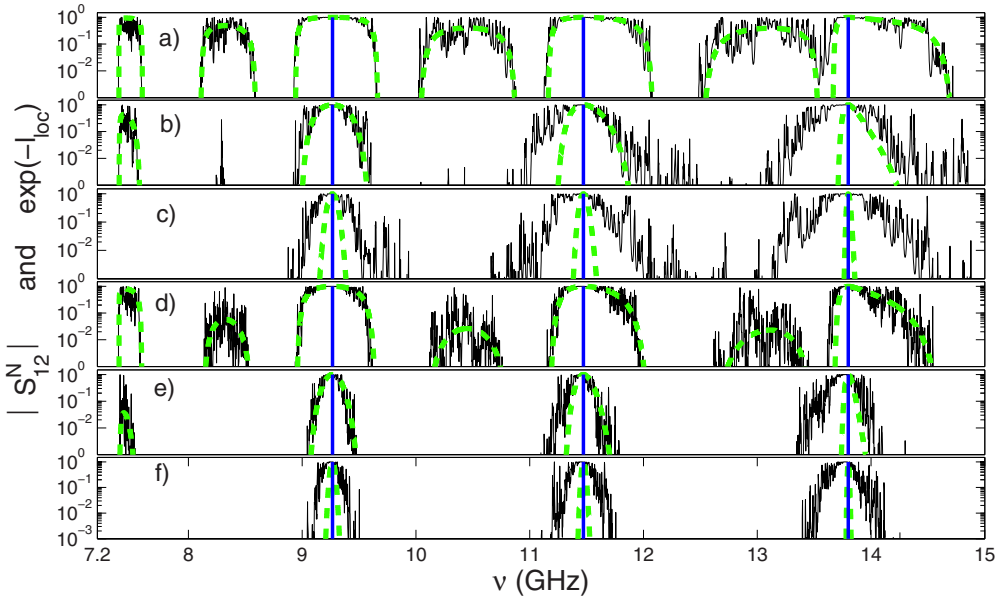

FIG. 5. (Color online) Transmission spectrum $|S_{12}^N|$ (solid curves) and $\exp(-l_{loc})$ (dashed curves) for $N=100$ and $N=400$: (a)–(c) $N=100$ cells; (a) weak, (b) medium, and (c) strong disorder. (d)–(f) $N=400$ cells; (d) weak, (e) medium, and (f) strong disorder.

V. LOCALIZATION LENGTH

In this section we derive an analytical expression for the *localization length* L_{loc} and relate it with the experimental data. In the case of weak positional disorder,

$$(k_a\sigma)^2 \ll 1, \tag{5.1}$$

an analytical expression for this quantity can be obtained as follows. First, we expand the transfer matrix $Q(n)$ defined by Eq. (2.9), up to quadratic terms in the perturbation parameter $k_a\sigma\eta(n)$,

$$\hat{Q}(n) \approx \left\{1 - \frac{(k_a\sigma)^2\eta^2(n)}{2}\right\}\hat{Q}^{(0)} + k_a\sigma\eta(n)\hat{Q}^{(1)}. \tag{5.2}$$

The unperturbed $\hat{Q}^{(0)}$ and first-order $\hat{Q}^{(1)}$ matrices are suitable to be presented in the form

$$\hat{Q}^{(0)} = \begin{pmatrix} u & v^* \\ v & u^* \end{pmatrix}, \quad \hat{Q}^{(1)} = \begin{pmatrix} iu & -iv^* \\ iv & -iu^* \end{pmatrix}, \tag{5.3a}$$

$$u = [\cos(k_b d_b) + i\alpha_+ \sin(k_b d_b)]\exp(ik_a d_a), \tag{5.3b}$$

$$v = i\alpha_- \sin(k_b d_b)\exp(ik_a d_a), \tag{5.3c}$$

$$\det \hat{Q}^{(0)} = \det \hat{Q}^{(1)} = |u|^2 - |v|^2 = 1. \tag{5.3d}$$

Also, it is useful for further calculations to take into account that the real and imaginary parts, $u_r \equiv \mathrm{Re}\, u$ and $u_i \equiv \mathrm{Im}\, u$, of the matrix element u can be expressed as

$$u_r = \cos(\kappa d), \quad u_i^2 = \sin^2(\kappa d) + |v|^2. \tag{5.4}$$

The first equality is identical to dispersion relation (2.16), while the second one is a direct consequence of matrix unimodularity (5.3d).

In order to extract the effects that are solely due to disorder, it is conventional to perform a canonical transformation to the Bloch normal-mode representation in transfer relation (2.8),

$$\begin{pmatrix} \tilde{A}_{n+1}^+ \\ \tilde{A}_{n+1}^- \end{pmatrix} = \hat{P}\hat{Q}\hat{P}^{-1}\begin{pmatrix} \tilde{A}_n^+ \\ \tilde{A}_n^- \end{pmatrix}, \tag{5.5a}$$

$$\begin{pmatrix} \tilde{A}_n^+ \\ \tilde{A}_n^- \end{pmatrix} = \hat{P}\begin{pmatrix} A_n^+ \\ A_n^- \end{pmatrix}. \tag{5.5b}$$

The transformation matrix $\hat{P}$ is specified in such a manner to make the unperturbed matrix $\hat{Q}^{(0)}$ diagonal,

$$\hat{P}\hat{Q}^{(0)}\hat{P}^{-1} = \begin{pmatrix} \exp(+i\kappa d) & 0 \\ 0 & \exp(-i\kappa d) \end{pmatrix}, \tag{5.6}$$

in complete accordance with the Floquet theorem[17], or the same, the Bloch condition[18]. The solution of the problem for the eigenvectors and eigenvalues of $\hat{Q}^{(0)}$ results in

$$\hat{P} = \begin{pmatrix} |v|/\beta_+ & -iv^*/\beta_- \\ iv/\beta_- & |v|/\beta_+ \end{pmatrix}, \tag{5.7a}$$

$$\beta_\pm^2 = 2\sqrt{1-u_r^2}(u_i \mp \sqrt{1-u_r^2}) = 2\,\sin(\kappa d)[u_i \mp \sin(\kappa d)], \tag{5.7b}$$

$$\beta_+^2\beta_-^2 = 4|v|^2\sin^2(\kappa d), \tag{5.7c}$$

$$\det \hat{P} = \det \hat{P}^{-1} = |v|^2(\beta_+^{-2} - \beta_-^{-2}) = 1. \tag{5.7d}$$

After substituting Eqs. (5.2), (5.3a), and (5.7a) into the canonical transfer relation (5.5a), one can obtain the explicit perturbative recursion relations for the new complex amplitudes,

$$\tilde{A}_{n+1}^+ = \left[1 - \frac{k_a^2\sigma^2\eta^2(n)}{2} + \frac{ik_a\sigma\eta(n)u_i}{\sin(\kappa d)}\right] \times \exp(i\kappa d)\tilde{A}_n^+ - \frac{k_a\sigma\eta(n)v^*}{\sin(\kappa d)}\exp(i\kappa d)\tilde{A}_n^-, \tag{5.8}$$

$$\tilde{A}_{n+1}^- = \left[1 - \frac{k_a^2\sigma^2\eta^2(n)}{2} - \frac{ik_a\sigma\eta(n)u_i}{\sin(\kappa d)}\right] \times \exp(-i\kappa d)\tilde{A}_n^- - \frac{k_a\sigma\eta(n)v}{\sin(\kappa d)}\exp(-i\kappa d)\tilde{A}_n^+. \tag{5.9}$$

Now one can see from these equations that one equation can be directly obtained from the other just by complex conjugation, if we suppose that $\tilde{A}_n^+ = \tilde{A}_n^{-*}$. In other words, it is convenient to seek the amplitudes $\tilde{A}_n^\pm$ in terms of action-angle variables,

$$\tilde{A}_n^\pm = R_n \exp(\pm i\theta_n). \tag{5.10}$$

In order to derive the equation for the real amplitude R_n, we multiply Eq. (5.8) by Eq. (5.9). Within the second order of approximation in the perturbation parameter $k_a\sigma\eta(n)$, we have

$$\frac{R_{n+1}^2}{R_n^2} = 1 + \frac{2k_a\sigma\eta(n)|v|}{\sin(\kappa d)}\sin(2\theta_n + k_a d_a) - k_a^2\sigma^2\eta^2(n) + \frac{k_a^2\sigma^2\eta^2(n)}{\sin^2(\kappa d)}[u_i^2 + |v|^2 + 2u_i|v|\cos(2\theta_n + k_a d_a)]. \tag{5.11}$$

The logarithm of Eq. (5.11), which determines the localization length, is also expanded within the quadratic approximation,

$$\ln\left(\frac{R_{n+1}^2}{R_n^2}\right) = \frac{2k_a\sigma\eta(n)|v|}{\sin(\kappa d)}\sin(2\theta_n + k_a d_a) + \frac{2k_a^2\sigma^2\eta^2(n)|v|^2}{\sin^2(\kappa d)} \times \left[1 - \sin^2(2\theta_n + k_a d_a) + \frac{u_i}{|v|}\cos(2\theta_n + k_a d_a)\right]. \tag{5.12}$$

Now we are in a position to write down the expression for the inverse localization length L_{loc}^{-1} that is known to be defined as follows[19]:

$$L_{\mathrm{loc}}^{-1} = \frac{1}{2d}\overline{\left\langle \ln\left(\frac{R_{n+1}^2}{R_n^2}\right)\right\rangle}. \tag{5.13}$$

The average $\langle ab\rangle$ is performed over the disorder $\eta(n)$ and the average $\overline{ab}$ is carried out over the rapid random phase θ_n. Within the accepted approximation and for *uncorrelated* disorder, see Eq. (2.2), we may regard the random quantities $\eta(n)$ and $\eta^2(n)$ to be uncorrelated with trigonometrical functions, containing the angle variable θ_n. Moreover, it can be shown (see, e.g., Ref. 19) that the distribution of phase θ_n, within the first order of approximation in a weak disorder, is homogeneous (the corresponding distribution function is constant). Therefore, after averaging over θ_n of Eq. (5.12), the term linear in $\eta(n)$ and the last term in the brackets vanish and $\sin^2(2\theta_n + k_a d_a)$ is replaced with 1/2. As a result, we get

$$L_{\mathrm{loc}}^{-1} = (k_a\sigma)^2 \frac{\alpha_-^2 \sin^2(k_b d_b)}{2d \sin^2(\kappa d)}. \tag{5.14}$$

This expression is in complete correspondence with that obtained in Refs. 11 and 20 using a different approach and reduces to Eq. (13) of Ref. 21 for the limiting case of delta-like barriers. The appearance of the term $\sin^2(k_b d_b)$ in the numerator of Eq. (5.14) indicates that at frequencies obeying the Teflon resonance condition $k_b d_b = m\pi$, the localization length turns into infinity. That is, the random array becomes transparent and this is what is observed in the experimental and numerical transmission coefficient plotted in Figs. 3–5.

As is known, the localization length is directly related to the transmittance T_N for a finite array of the length $L=Nd$ according to the famous relation $\langle \ln T_N\rangle = -2L/L_{\mathrm{loc}}$. In view of this relation and recalling that $T_N = |S_{12}^N|^2$, see Eq. (2.13), it is convenient to introduce the *rescaled* inverse localization length l_{loc}^{-1} as

$$\langle \ln|S_{12}^N|\rangle = -L/L_{\mathrm{loc}} \equiv -l_{\mathrm{loc}}^{-1}. \tag{5.15}$$

According to Eq. (5.14), one can get

$$l_{\mathrm{loc}}^{-1} = (\sigma/d)^2 F(\nu) N. \tag{5.16}$$

Here we introduced the form factor

$$F(\nu) = (k_a d)^2 \frac{\alpha_-^2 \sin^2(k_b d_b)}{2 \sin^2(\kappa d)} \tag{5.17}$$

that specifies the frequency profile of the inverse localization length and is determined only by the parameters of the underlying regular array. The rescaled inverse localization length, Eq. (5.16), increases linearly with the number of cells N and quadratically with the amount of disorder σ/d.

In Fig. 6(a), we plot the form factor $F(\nu)$ for the parameters of our system, $d_a = d_b = 4.078$ cm, $n_a = 1$, and $n_b = \sqrt{2.08}$. In Fig. 6(b), we present the frequency dependence of l_{loc}^{-1} for an array of 400 cells for the cases of weak, medium, and strong disorder. These figures show that the attenuation of transmission is larger for the sixth band and least for the first band, and that the states are completely extended at the Teflon resonances.

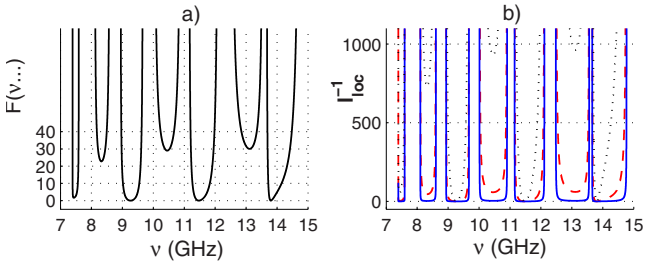

FIG. 6. (Color online) (a) Form factor $F(\nu, d_a, d_b, n_a, n_b)$ for $d_a = d_b = 4.078$ cm, $n_a = 1$, and $n_b = \sqrt{2.08}$; (b) inverse localization length l_{loc}^{-1} for $N=400$ for weak (solid curve), medium (dashed curve), and strong (dotted curve) disorder.

In order to compare our analytical results with the experimental and numerical ones, we define the theoretical value $|S_{12}^N|_{\mathrm{th}}$ of the transmission spectrum as follows:

$$|S_{12}^N|_{\mathrm{th}} \equiv \exp(-l_{\mathrm{loc}}^{-1}) = \exp[-(\sigma/d)^2 F(\nu) N]. \tag{5.18}$$

This is what is plotted in green dashed lines in Fig. 4 for the cases of weak, medium, and strong disorder in the $N=26$ cells array and in Fig. 5 for the array with $N=100$ and $N=400$.

Inspection of Figs. 4 and 5 reveals that the theoretical expression for the transmission spectrum provides a very good description for the case of weak disorder for the whole range of frequencies. For medium disorder, the agreement is moderate but only up to the region of the first resonance band. The higher the frequency the higher the discrepancy, in accordance with the range of validity (5.1) of expression (5.16), namely, $(k_a\sigma)^2 \ll 1$.

We would like to stress that the *statistically averaged* analytical results of this section required the structure to be sufficiently long. Therefore, a better correspondence with numerics and experiment is expected for longer samples. The data in Figs. 4 and 5 confirm this fact. Indeed, by comparing Figs. 4 and 5, we see that the larger the number of cells in the array, the better the agreement between the numerical simulations [transfer matrix calculations (2.12)] and expression (5.18). Moreover, the quantity $\exp(-l_{\mathrm{loc}}^{-1})$ gives a good fit to the numerical data even for the case of medium disorder and up to $\nu = 11.5$ GHz. Observe also that already for $N=100$ the nonresonance bands have completely disappeared for the medium disorder case.

VI. SUMMARY

We have analyzed experimentally and theoretically the effects of positional disorder in the 1D Kronig-Penney model formed by a finite number of two alternating dielectric slabs, focusing on the transmission for weak, medium, and strong uncorrelated disorder. Our results can be divided in two parts. In the first part, we show that in spite of the absorption by the metallic walls of the microwave Kronig-Penney experiment, the numerical simulations, based on the transfer matrix multiplication (2.13), describe the experimental transmission for weak, medium, and strong disorder. As expected, there is complete transparency (transmission coefficient

equals 1) at the Teflon resonances for any amount of disorder. Surprisingly, however, localization is strongly inhibited in a large neighborhood of these resonances. That is, we found that the so-called resonance bands survive even for relatively strong disorder and large number of cells, whereas the nonresonance transmission bands disappear already for relatively weak disorder. The structured similarity between experimental and numerical data can be explained by the distinct nature of absorption and resonance effects. Namely, the latter is due to coherent effects, in contrast with the noncoherent nature of absorption.

In the second part of our study, we derived an analytical expression for the average transmission coefficient, Eq. (5.18), under the assumption of weak disorder and for finite number of cells. To do this, we used the relation between the transmission coefficient and the localization length that involves the finite size of samples and applied it to the experimental situation. As a result, we found that the analytical expression for the transmission coefficient reproduces quite well the frequency dependence of the experimentally obtained data for weak disorder. Note again that the global correspondence between analytical and experimental results occurs in the presence of absorption that is unavoidable experimentally. In addition, transfer matrix calculations for larger arrays (not realizable in our experimental setup) showed that this analytical expression is valid even for medium disorder up to a certain frequency. In the limit of an infinitely long array, and for any amount of disorder, the transmission spectrum is a set of delta peaks at the Teflon resonances. Thus, from the above-mentioned correspondence, we conclude that the expression for the localization length (5.14) is a working quantity for finite samples, a fact that is not commonly used in applications.

The method we used to derive the expression for the localization length can be generalized to a more general case of the correlated disorder,[14,15,20–26] for which anomalous effects in the transmission are predicted and experimentally observed. Our results can be applied also to photonic crystals and electron superlattices, as well as to the propagation of acoustic waves in disordered systems.

ACKNOWLEDGMENTS

G.A.L-A. acknowledges support from CONACyT, convenio Grant No. P51458. and from the DFG via the Mercator Professorship program. F.M.I. acknowledges financial support from CONACyT Grant No. F2030, and U.K. and H.J.S. from the Deutsche Forschungsgemeinschaft via the Forschergruppe 760 "Scattering Systems with Complex Dynamics."

[1] *Wave Propagation: From Electrons to Photonic Crystals and Left-Handed Materials*, edited by P. Markoš and C. M. Soukoulis (Princeton University Press, Princeton, NJ, 2008).
[2] A. R. McGurn, K. T. Christensen, F. M. Mueller, and A. A. Maradudin, Phys. Rev. B **47**, 13120 (1993).
[3] D. R. Smith, W. J. Padilla, D. C. Vier, S. C. Nemat-Nasser, and S. Schultz, Phys. Rev. Lett. **84**, 4184 (2000).
[4] R. A. Shelby, D. R. Smith, and S. Schultz, Science **292**, 77 (2001).
[5] C. G. Parazzoli, R. B. Greegor, K. Li, B. E. C. Koltenbah, and M. Tanielian, Phys. Rev. Lett. **90**, 107401 (2003).
[6] A. Esmailpour, M. Esmaeilzadeh, E. Faizabadi, P. Carpena, and M. R. R. Tabar, Phys. Rev. B **74**, 024206 (2006).
[7] D. Nau, A. Schönhardt, C. Bauer, A. Christ, T. Zentgraf, J. Kuhl, M. W. Klein, and H. Giessen, Phys. Rev. Lett. **98**, 133902 (2007).
[8] I. V. Ponomarev, M. Schwab, G. Dasbach, M. Bayer, T. L. Reinecke, J. P. Reithmaier, and A. Forchel, Phys. Rev. B **75**, 205434 (2007).
[9] A. A. Asatryan, L. C. Botten, M. A. Byrne, V. D. Freilikher, S. A. Gredeskul, I. V. Shadrivov, R. C. McPhedran, and Y. S. Kivshar, Phys. Rev. Lett. **99**, 193902 (2007).
[10] H. Dong and S.-J. Xiong, J. Phys.: Condens. Matter **10**, 7691 (1998).
[11] V. Baluni and J. Willemsen, Phys. Rev. A **31**, 3358 (1985).
[12] G. A. Luna-Acosta, H. Schanze, U. Kuhl, and H.-J. Stöckmann, New J. Phys. **10**, 043005 (2008).
[13] U. Kuhl and H.-J. Stöckmann, Phys. Rev. Lett. **80**, 3232 (1998).
[14] U. Kuhl, F. M. Izrailev, A. A. Krokhin, and H.-J. Stöckmann, Appl. Phys. Lett. **77**, 633 (2000).
[15] A. Krokhin, F. Izrailev, U. Kuhl, H.-J. Stöckmann, and S. E. Ulloa, Physica E (Amsterdam) **13**, 695 (2002).
[16] U. Kuhl, F. M. Izrailev, and A. A. Krokhin, Phys. Rev. Lett. **100**, 126402 (2008).
[17] G. Floquet, Ann. Sci. Ec. Normale Super. **12**, 47 (1883).
[18] F. Bloch, Z. Phys. A **52**, 555 (1929).
[19] F. M. Izrailev, S. Ruffo, and L. Tessieri, J. Phys. A **31**, 5263 (1998).
[20] F. M. Izrailev and N. M. Makarov, Phys. Rev. Lett. **102**, 203901 (2009).
[21] F. M. Izrailev, A. A. Krokhin, and S. E. Ulloa, Phys. Rev. B **63**, 041102(R) (2001).
[22] F. M. Izrailev and A. A. Krokhin, Phys. Rev. Lett. **82**, 4062 (1999).
[23] F. M. Izrailev and N. M. Makarov, Opt. Lett. **26**, 1604 (2001).
[24] F. M. Izrailev and N. M. Makarov, Appl. Phys. Lett. **84**, 5150 (2004).
[25] F. M. Izrailev and N. M. Makarov, J. Phys. A **38**, 10613 (2005).
[26] J. C. Hernández Herrejón, F. M. Izrailev, and L. Tessieri, Physica E (Amsterdam) **40**, 3137 (2008).